Appl. Math. Mech. -Engl. Ed., **40**(7), 1017–1028 (2019)

Applied Mathematics and Mechanics (English Edition)

https://doi.org/10.1007/s10483-019-2501-8

Rotating electroosmotic flows in soft parallel plate microchannels*

Yongbo LIU, Yongjun JIAN†

School of Mathematical Science, Inner Mongolia University, Hohhot 010021, China

(Received Oct. 8, 2018 / Revised Dec. 9, 2018)

Abstract We present a theoretical investigation of rotating electroosmotic flows (EOFs) in soft parallel plate microchannels. The soft microchannel, also called as the polyelectrolyte-grafted microchannel, is denoted as a rigid microchannel coated with a polyelectrolyte layer (PEL) on its surface. We compare the velocity in a soft microchannel with that in a rigid one for different rotating frequencies and find that the PEL has a trend to lower the velocities in both directions for a larger equivalent electrical double layer (EDL) thickness λ_{FCL} ($\lambda_{\mathrm{FCL}} = 0.3$) and a smaller rotating frequency ω ($\omega < 5$). However, for a larger rotating frequency ω ($\omega = 5$), the main stream velocity u far away from the channel walls in a soft microchannel exceeds that in a rigid one. Inspired by the above results, we can control the EOF velocity in micro rotating systems by imparting PELs on the microchannel walls, which may be an interesting application in biomedical separation and chemical reaction.

Key words rotating electroosmotic flow (EOF), soft microchannel, polyelectrolyte layer (PEL) thickness

Chinese Library Classification O363.2
2010 Mathematics Subject Classification 76A99, 76W05

1 Introduction

Recently, the advancement in the investigation of electrokinetic phenomena in microfluidic systems promotes diverse applications of such systems in medicine, energy conversion, and analytical chemistry[1–2]. The driving mechanisms for fluid flows in microchannels include the electric field[3–7], pressure gradients[8], electromagnetic field[9–20], light[21], and acoustic wave[22]. Among these different micropumps, the electroosmotic flow, driven purely by the electrical field, has attracted many researchers' attention due to better flow control.

When an electrolyte fluid is brought into contact with a solid surface, the surface and the electrolyte fluid often get oppositely charged due to the electrolyte chemical processes, which gives rise to the electrical double layer (EDL)[23]. Therefore, when we impose an electric field along the tangential direction of the charged surface, the net charges in the electrolyte fluid will

* Citation: LIU, Y. B. and JIAN, Y. J. Rotating electroosmotic flows in soft parallel plate microchannels. *Applied Mathematics and Mechanics* (*English Edition*), **40**(7), 1017–1028 (2019) https://doi.org/10.1007/s10483-019-2501-8

† Corresponding author, E-mail: jianyj@imu.edu.cn

Project supported by the National Natural Science Foundation of China (Nos. 11772162 and 11472140), the Inner Mongolia Autonomous Region Grassland Talent (No. 12000-12102013), and the Natural Science Foundation of Inner Mongolia Autonomous Region of China (No. 2016MS0106)

move under the action of the electric field force. Then, the migration of the net charges will carry the electrolyte solution along with them by viscosity. Such flow is known as the electroosmotic flow (EOF)[24]. In practical applications, such as mass separation or flow control in centrifuges, the system is situated in a rotating environment[25–26]. Rotating flows may be used in compact disc (CD)-based centrifugal microfluidics, in which the driving force is the centrifugal force. This system enables us to conduct in parallel a great many fluid flow assays[27], which is one of the most important advantages of such a rotating system. In addition, Wang et al.[28] demonstrated that this system could effectively lower chemical reaction, Joule heat generation and ion concentration variation. Martinez-Duarte et al.[29] and Boettcher et al.[30] studied the electrophoresis phenomenon in a rotating microfluidic system. Duffy et al.[31] experimentally investigated the electrokinetic flow, driven by the centrifugal force, in a rotational system. The analysis of the rotating EOF in microfluidic systems is of essential importance and has become a new topic of the research recently.

By using a Newtonian fluid, Chang and Wang[32] pioneered the investigation of the steady rotating EOF in microfluidic systems. Under the Debye-Hückel approximation condition, they obtained the analytical expressions of the flow velocity. Their result showed that the transverse flow velocity v achieved its maximum value at $\omega = 1$ (ω denotes the nondimensional rotating frequency). Then, Si et al.[33] and Gheshlaghi et al.[34] analyzed the transient rotating EOF of a Newtonian fluid in a microchannel almost at the same time by using two different methods, respectively. Their theory was extended by Xie and Jian[35] by considering the high zeta potential condition and a non-Newtonian fluid. They found that, for a larger rotating angular velocity, the velocity direction is altered by the Coriolis force significantly. The corresponding model for a rectangular microchannel was developed by Ng and Qi[36]. It was demonstrated that the rotating speed of the system had an unequal effect on the fluid flow for different zeta potential distributions or different channel widths. Considering the slip boundary condition of velocity, Shit et al.[37] numerically studied the rotating EOF through slowly varying microchannels. They compared their numerical results with the reported theoretical results, and good agreement was found.

Recently, the EOF in soft micro/nanochannels has attracted remarkable attention. A micro/nanochannel with walls coated with the polyelectrolyte layer (PEL) is called a soft micro/nanochannel[38–40], which frequently happens when considering biological surfaces[41]. The PEL contains a kind of ion with a fixed charge density and thus it can be defined as a fixed charge layer (FCL). The presence of this PEL has twofold effects on the EOF. Firstly, the fixed charge in the PEL affects the electrostatic potential in the EDL. Secondly, the PEL will impose an additional resistance to the flow[40]. The soft nanochannel can be used in energy conversion systems, cell membranes[42], and transistors and diodes[43]. Donath and Voigt[41] first provided a theoretical model of the electrokinetic flow in a soft nanochannel. Then, Matin and Ohshima[44] studied the mixed pressure driven and the EOF in soft nanochannels. Chanda et al.[45] and Chen and Das[46] investigated the streaming potential in a soft nanochannel for low and high zeta potentials, respectively. Very recently, the EOF in soft microchannels has also received attention of some scholars. The pioneering work of the EOF in soft microchannels was conducted by Hoshyargar et al.[47]. They investigated the detailed hydrodynamic dispersion characteristics of a neutrally charged solute by the EOF in soft microchannels. Their results revealed that the grafted PEL could increase the hydrodynamic dispersion of the EOF. Then, Sadeghi[48] theoretically studied the EOF in a soft rectangular microchannel. In addition, other important applications of the soft microchannel include the experimental works of droplet generation by Pang et al.[49] and droplet coalescence by Liu et al.[50].

To the authors' best knowledge, although considerable attention has been paid to the rotating EOF and EOF through a soft microchannel, respectively, the effect of rotation on the EOF in a soft microchannel has not been reported yet, which may be an important case in biomedical separation and chemical reaction. Thus, the present work is devoted to filling this

gap. Analytical solutions of the velocity and volume flow rate are provided in Section 2. The influences of the corresponding non-dimensional parameters on the EOF velocity distributions are discussed in Section 3. The main results are summarized in Section 4.

2 Mathematical formulations

As depicted in Fig. 1, we consider the rotating EOF in a soft parallel plate microchannel of height $2h$. The electrolyte solution in the channel is taken as an incompressible Newtonian fluid. We set up a Cartesian coordinate system (x^*, y^*, z^*) at the microchannel centerline, where the x^*-axis is along the channel, the y^*-axis points along the transverse direction, and the z^*-axis runs vertically upwards. An electric field with the magnitude E_0 is imposed along the positive x^*-direction to actuate the fluid flow. Meanwhile, the above microchannel rotates about the z^*-axis at a constant angular frequency Ω. The thickness of the ion-penetrable charged PEL, containing positively charged FCL ions, is $d^*(< h)$. It is assumed that the zeta potential is low enough so that the Debye-Hückel approximation is applicable. In addition, we also assume that the permittivity of the medium is identical within and outside the PEL[45]. Due to the symmetry of the fluid flow, we only need to consider the channel bottom half $(-h \leqslant z^* \leqslant 0)$. The PEL (the bulk fluid layer) is denoted as the region $-h \leqslant z^* \leqslant -h + d^* (-h + d^* \leqslant z^* \leqslant 0)$.

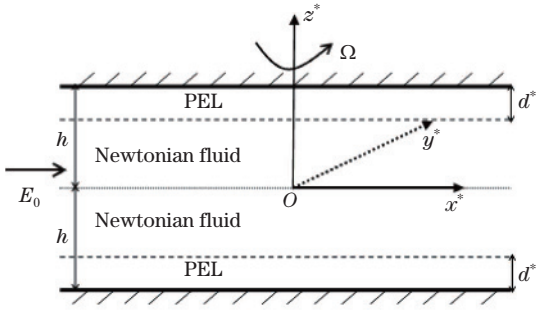

Fig. 1 Schematic illustration of the rotating EOF in a soft microchannel

2.1 The electrostatic potential in the EDL

According to the electrostatics theory, the governing equations (within PEL and bulk fluid layer, respectively) for the electrostatic potential distribution are given as

$$\frac{\mathrm{d}^2\psi^*}{\mathrm{d}z^{*2}} = -\frac{em(n_+ - n_-)}{\varepsilon_0\varepsilon_\mathrm{r}}, \quad -h + d^* \leqslant z^* \leqslant 0, \tag{1}$$

$$\frac{\mathrm{d}^2\psi^*}{\mathrm{d}z^{*2}} = -\frac{em(n_+ - n_-) + ZeN}{\varepsilon_0\varepsilon_\mathrm{r}}, \quad -h \leqslant z^* \leqslant -h + d^*, \tag{2}$$

where ψ^* denotes the electrostatic potential, e stands for the electric charge, m represents the valence, $\varepsilon_0\varepsilon_\mathrm{r}$ is the permittivity of the fluid, $n_+ (n_-)$ is known as the cations (anions) number density, Z is the FCL ions valence, and N represents the FCL ions number density. The influence of the FCL ions on the electrostatic potential distribution is shown in Eq. (2). Consider an electrolyte kept in a soft microchannel, and the electrolyte ions in it are assumed to satisfy the Boltzmann distribution, which is expressed as $n_\pm = n_\infty \exp(\mp(em\psi^*)/(k_\mathrm{B}T))$[47]. In addition, for the assumed small enough electrical potential, we can employ the Debye-Hückel approximation. Therefore, the above governing equations are rewritten as

$$\frac{\mathrm{d}^2\psi^*}{\mathrm{d}z^{*2}} = \frac{\psi^*}{\lambda^{*2}}, \quad -h + d^* \leqslant z^* \leqslant 0, \tag{3}$$

$$\frac{\mathrm{d}^2\psi^*}{\mathrm{d}z^{*2}}=\frac{\psi^*}{\lambda^{*2}}-\frac{\psi_\mathrm{s}}{\lambda^{*2}_\mathrm{FCL}},\quad -h\leqslant z^*\leqslant -h+d^*, \tag{4}$$

where $\lambda^*=(\varepsilon_0\varepsilon_\mathrm{r}k_\mathrm{B}T/(2n_\infty e^2m^2))^{1/2}$ and $\lambda^*_\mathrm{FCL}=(\varepsilon_0\varepsilon_\mathrm{r}k_\mathrm{B}T/(Ne^2mZ))^{1/2}$ are the traditional EDL thickness and the equivalent EDL thickness, respectively[45]. $\psi_\mathrm{s}=k_\mathrm{B}T/(em)$ is the characteristic scale of the electrostatic potential. n_∞ is the bulk ionic number density, and $k_\mathrm{B}T$ denotes the thermal energy[45]. The following boundary conditions are used to solve Eqs. (3) and (4):

$$\begin{cases}\dfrac{\mathrm{d}\psi^*}{\mathrm{d}z^*}\Big|_{z^*=0}=0,\quad \psi^*\,|_{z^*=(-h+d^*)^+}=\psi^*\,|_{z^*=(-h+d^*)^-},\\ \dfrac{\mathrm{d}\psi^*}{\mathrm{d}z^*}\Big|_{z^*=(-h+d^*)^+}=\dfrac{\mathrm{d}\psi^*}{\mathrm{d}z^*}\Big|_{z^*=(-h+d^*)^-},\quad \psi^*\,|_{z^*=-h}=\zeta^*.\end{cases} \tag{5}$$

In Eq. (5), the first condition implies the symmetry of the electrical potential about the z^*-axis. The second condition represents the continuity of the electrical potential at the FCL-bulk electrolyte interface, and the third condition represents the continuity of the electrical field at the FCL-bulk electrolyte interface. In addition, the last condition provides the electrical potential at the wall, known as the electric zeta potential. The following normalization variables are introduced to non-dimensionalize the equations:

$$z=\frac{z^*}{h},\quad \lambda=\frac{\lambda^*}{h},\quad d=\frac{d^*}{h},\quad \lambda_\mathrm{FCL}=\frac{\lambda^*_\mathrm{FCL}}{h},\quad \psi=\frac{\psi^*}{\psi_\mathrm{s}},\quad \zeta=\frac{\zeta^*}{\psi_\mathrm{s}}. \tag{6}$$

According to the above defined dimensionless variables, Eqs. (3), (4), and (5) are simplified to

$$\frac{\mathrm{d}^2\psi}{\mathrm{d}z^2}-\frac{\psi}{\lambda^2}=0,\quad -1+d\leqslant z\leqslant 0, \tag{7}$$

$$\frac{\mathrm{d}^2\psi}{\mathrm{d}z^2}-\frac{\psi}{\lambda^2}=-\frac{1}{\lambda^2_\mathrm{FCL}},\quad -1\leqslant z\leqslant -1+d, \tag{8}$$

$$\begin{cases}\dfrac{\mathrm{d}\psi}{\mathrm{d}z}\Big|_{z=0}=0,\quad \psi\,|_{z=(-1+d)^+}=\psi\,|_{z=(-1+d)^-},\\ \dfrac{\mathrm{d}\psi}{\mathrm{d}z}\Big|_{z=(-1+d)^+}=\dfrac{\mathrm{d}\psi}{\mathrm{d}z}\Big|_{z=(-1+d)^-},\quad \psi\,|_{z=-1}=\zeta.\end{cases} \tag{9}$$

The analytical solutions for the electrostatic potential distributions are given as

$$\psi=\frac{1}{\cosh(1/\lambda)}(K^2\cosh(d/\lambda)+\zeta-K^2)\cosh\Big(\frac{z}{\lambda}\Big),\quad -1+d\leqslant z\leqslant 0, \tag{10}$$

$$\psi=K^2\Big(1-\frac{\sinh D}{\cosh(1/\lambda)}\sinh\Big(\frac{z+1}{\lambda}\Big)\Big)+\frac{\zeta-K^2}{\cosh(1/\lambda)}\cosh\Big(\frac{z}{\lambda}\Big),\quad -1\leqslant z\leqslant -1+d, \tag{11}$$

where $D=(1-d)/\lambda$, and $K{=}\lambda/\lambda_\mathrm{FCL}$.

2.2 Distributions of the velocity fields

For an incompressible fluid, the steady EOF velocity between two slit soft microchannels satisfies the following continuity equation (see Eq. (12)). In addition, in the rotating coordinate system with the angular velocity $\boldsymbol{\Omega}=(0,0,\Omega)$, the velocity satisfies the modified Cauchy momentum equation[30],

$$\nabla\cdot\boldsymbol{V}=0, \tag{12}$$

$$\rho^*(\boldsymbol{V}\cdot\nabla\boldsymbol{V}+2\boldsymbol{\Omega}\times\boldsymbol{V})=-\nabla P^*+\mu^*\nabla^2\boldsymbol{V}+\boldsymbol{f}, \tag{13}$$

where ρ^* is the fluid density, and μ^* and $\boldsymbol{V}=(u^*,v^*,w^*)$ are the dynamic viscosity and velocity vector, respectively. $P^*=p^*-\rho^*|\boldsymbol{\Omega}\times\boldsymbol{r}|^2/2$ denotes the modified pressure, and $\boldsymbol{r}=(x^*,y^*,z^*)$ is the position vector. The last term $\boldsymbol{f}$ in Eq. (13) is the body force. For fully developed flows, the axial and the transverse velocities u^* and v^* depend on z^* only. Moreover, the continuity equation is satisfied automatically. The body force $\boldsymbol{f}$ is defined as

$$\boldsymbol{f}=(-\rho_{\mathrm{e}}E_0,0,0)\quad\text{with}\quad\rho_{\mathrm{e}}=-\varepsilon_0\varepsilon_{\mathrm{r}}\frac{\mathrm{d}^2\psi^*}{\mathrm{d}z^{*2}}. \tag{14}$$

As we have mentioned above, an additional resistive force is present within the PEL. The magnitudes of the resistive force in such a soft microchannel, resembling the Darcy model, are $\mu_{\mathrm{c}}u^*$ and $\mu_{\mathrm{c}}v^*$, where μ_{c} is the drag coefficient (per unit volume)[44]. Therefore, the Cauchy momentum equations in soft microchannels are reduced to

$$-2\rho^*\Omega v^*=\varepsilon_0\varepsilon_{\mathrm{r}}E_0\frac{\mathrm{d}^2\psi^*}{\mathrm{d}z^{*2}}+\mu^*\frac{\mathrm{d}^2u^*}{\mathrm{d}z^{*2}},\quad 2\rho^*\Omega u^*=\mu^*\frac{\mathrm{d}^2v^*}{\mathrm{d}z^{*2}},\quad -h+d^*\leqslant z^*\leqslant 0, \tag{15}$$

$$-2\rho^*\Omega v^*=\varepsilon_0\varepsilon_{\mathrm{r}}E_0\frac{\mathrm{d}^2\psi^*}{\mathrm{d}z^{*2}}-\mu_{\mathrm{c}}u^*+\mu^*\frac{\mathrm{d}^2u^*}{\mathrm{d}z^{*2}},\ 2\rho^*\Omega u^*=\mu^*\frac{\mathrm{d}^2v^*}{\mathrm{d}z^{*2}}-\mu_{\mathrm{c}}v^*,\ -h\leqslant z^*\leqslant -h+d^*. \tag{16}$$

To simplify the analysis procedure, the following dimensionless parameters are introduced:

$$u=\frac{u^*}{U_{\mathrm{eo}}},\quad v=\frac{v^*}{U_{\mathrm{eo}}},\quad U_{\mathrm{eo}}=\frac{\varepsilon_0\varepsilon_{\mathrm{r}}E_0\psi_{\mathrm{s}}}{\mu},\quad \omega=\frac{\rho\Omega h^2}{\mu},\quad \alpha=h\sqrt{\frac{\mu_{\mathrm{c}}}{\mu}}, \tag{17}$$

where U_{eo} is the classical EOF velocity scale in the absence of the rotating effect, ω is the nondimensional frequency in the rotating frame, and α denotes the normalized drag coefficient. Substituting these dimensionless parameters defined in Eq. (17) into Eqs. (15) and (16), we get the nondimensional Cauchy momentum equations as

$$\frac{\mathrm{d}^2u}{\mathrm{d}z^2}+2\omega v=-\frac{\psi}{\lambda^2},\quad 2\omega u=\frac{\mathrm{d}^2v}{\mathrm{d}z^2},\quad -1+d\leqslant z\leqslant 0, \tag{18}$$

$$\frac{\mathrm{d}^2u}{\mathrm{d}z^2}+2\omega v-\alpha^2u=-\frac{\psi}{\lambda^2},\quad 2\omega u=\frac{\mathrm{d}^2v}{\mathrm{d}z^2}-\alpha^2v,\quad -1\leqslant z\leqslant -1+d. \tag{19}$$

To seek the analytical solutions of Eqs. (18) and (19), we introduce a complex function $\chi(z)=u(z)+\mathrm{i}v(z)$, in which i denotes the imaginary unit. Thus, the hydrodynamic equations (18) and (19) can be substituted by the following complex differential equations:

$$\frac{\mathrm{d}^2\chi}{\mathrm{d}z^2}-2\omega\mathrm{i}\chi=-\frac{\psi}{\lambda^2},\quad -1+d\leqslant z\leqslant 0, \tag{20}$$

$$\frac{\mathrm{d}^2\chi}{\mathrm{d}z^2}-(2\omega\mathrm{i}+\alpha^2)\chi=-\frac{\psi}{\lambda^2},\quad -1\leqslant z\leqslant -1+d. \tag{21}$$

The appropriate boundary conditions for Eqs. (20) and (21) are

$$\begin{cases}\dfrac{\mathrm{d}\chi}{\mathrm{d}z}\Big|_{z=0}=0,\quad \chi\Big|_{z=(-1+d)^+}=\chi\Big|_{z=(-1+d)^-},\\ \dfrac{\mathrm{d}\chi}{\mathrm{d}z}\Big|_{z=(-1+d)^+}=\dfrac{\mathrm{d}\chi}{\mathrm{d}z}\Big|_{z=(-1+d)^-},\quad \chi\Big|_{z=-1}=0.\end{cases} \tag{22}$$

Physically, the first boundary condition implies that the velocity is symmetric, and the second (third) condition in Eq. (22) represents that the velocity (shear stress) is continuous at the FCL-bulk electrolyte interface. The fourth condition represents that the velocity is under the no-slip

boundary condition. Combining Eqs. (10), (11) and Eqs. (20)–(22), the analytical solutions of the velocity are finally obtained as

$$\chi(z)=B_1\cosh(\sqrt{2\omega\mathrm{i}}z)+\frac{\cosh(z/\lambda)}{(2\omega\mathrm{i}\lambda^2-1)\cosh(1/\lambda)}\Big(K^2\cosh\Big(\frac{d}{\lambda}\Big)+\zeta-K^2\Big),\quad -1+d\leqslant z\leqslant 0, \tag{23}$$

$$\begin{aligned}\chi(z)=&B_3\cosh(\sqrt{2\omega\mathrm{i}+\alpha^2}z)+B_4\sinh(\sqrt{2\omega\mathrm{i}+\alpha^2}z)+\frac{1}{(1-(\alpha^2+2\omega\mathrm{i})\lambda^2)\cosh(1/\lambda)}\\&\cdot\Big(K^2\sinh D\sinh\Big(\frac{z+1}{\lambda}\Big)+(K^2-\zeta)\cosh\Big(\frac{z}{\lambda}\Big)\Big)+\frac{K^2}{(2\omega\mathrm{i}+\alpha^2)\lambda^2},\quad -1\leqslant z\leqslant -1+d,\end{aligned} \tag{24}$$

where B_1, B_3, and B_4 are constants, and their expressions are given as follows:

$$\begin{aligned}B_1=&\frac{1}{\sqrt{2\omega\mathrm{i}}\sinh(\sqrt{2\omega\mathrm{i}}(-1+d))\cosh(\sqrt{2\omega\mathrm{i}+\alpha^2})}\Big(\sqrt{2\omega\mathrm{i}+\alpha^2}\cosh(\sqrt{2\omega\mathrm{i}+\alpha^2}d)B_4\\&+\frac{\sqrt{2\omega\mathrm{i}+\alpha^2}\sinh(\sqrt{2\omega\mathrm{i}+\alpha^2}(-1+d))(\zeta-K^2)}{1-(\alpha^2+2\omega\mathrm{i})\lambda^2}-\frac{\alpha^2\lambda\cosh(\sqrt{2\omega\mathrm{i}+\alpha^2})\sinh D}{(1-(\alpha^2+2\omega\mathrm{i})\lambda^2)\cosh(1/\lambda)(2\omega\mathrm{i}\lambda^2-1)}\\&\cdot\Big(K^2\cosh\Big(\frac{d}{\lambda}\Big)+\zeta-K^2\Big)-\frac{K^2\sqrt{2\omega\mathrm{i}+\alpha^2}\sinh(\sqrt{2\omega\mathrm{i}+\alpha^2}(-1+d))}{(2\omega\mathrm{i}+\alpha^2)\lambda^2}\Big),\end{aligned} \tag{25}$$

$$B_3=\frac{1}{\cosh(\sqrt{2\omega\mathrm{i}+\alpha^2})}\Big(B_4\sinh(\sqrt{2\omega\mathrm{i}+\alpha^2})+\frac{\zeta-K^2}{1-(\alpha^2+2\omega\mathrm{i})\lambda^2}-\frac{K^2}{(2\omega\mathrm{i}+\alpha^2)\lambda^2}\Big), \tag{26}$$

$$\begin{aligned}B_4=&\Big(\frac{\sqrt{2\omega\mathrm{i}}\sinh(\sqrt{2\omega\mathrm{i}}(-1+d))\cosh\sqrt{2\omega\mathrm{i}+\alpha^2}}{(1-(\alpha^2+2\omega\mathrm{i})\lambda^2)\cosh(1/\lambda)}\Big(K^2\sinh D\sinh\Big(\frac{d}{\lambda}\Big)+(K^2-\zeta)\cosh D\Big)\\&-\frac{\sqrt{2\omega\mathrm{i}}\sinh(\sqrt{2\omega\mathrm{i}}(-1+d))\cosh\sqrt{2\omega\mathrm{i}+\alpha^2}\cosh D}{(2\omega\mathrm{i}\lambda^2-1)\cosh(1/\lambda)}\Big(K^2\cosh\Big(\frac{d}{\lambda}\Big)+\zeta-K^2\Big)\\&+\sqrt{2\omega\mathrm{i}}\sinh(\sqrt{2\omega\mathrm{i}}(-1+d))\cosh(\sqrt{2\omega\mathrm{i}+\alpha^2}(-1+d))\Big(\frac{\zeta-K^2}{1-(\alpha^2+2\omega\mathrm{i})\lambda^2}-\frac{K^2}{(2\omega\mathrm{i}+\alpha^2)\lambda^2}\Big)\\&+\frac{K^2\sqrt{2\omega\mathrm{i}}}{(\alpha^2+2\omega\mathrm{i})\lambda^2}\sinh(\sqrt{2\omega\mathrm{i}}(-1+d))\cosh(\sqrt{2\omega\mathrm{i}+\alpha^2})-\cosh(\sqrt{2\omega\mathrm{i}}(-1+d))\\&\cdot\Big(\frac{\sqrt{2\omega\mathrm{i}+\alpha^2}\sinh(\sqrt{2\omega\mathrm{i}+\alpha^2}(-1+d))(\zeta-K^2)}{1-(\alpha^2+2\omega\mathrm{i})\lambda^2}\\&-\frac{\alpha^2\lambda\sinh D\cosh(\sqrt{2\omega\mathrm{i}+\alpha^2})}{(2\omega\mathrm{i}\lambda^2-1)(1-(\alpha^2+2\omega\mathrm{i})\lambda^2)\cosh(1/\lambda)}\Big(K^2\cosh\Big(\frac{d}{\lambda}\Big)+\zeta-K^2\Big)\\&-\frac{K^2\sqrt{2\omega\mathrm{i}+\alpha^2}\sinh(\sqrt{2\omega\mathrm{i}+\alpha^2}(-1+d))}{(2\omega\mathrm{i}+\alpha^2)\lambda^2}\Big)\Big)\Big/\Big(\sqrt{2\omega\mathrm{i}+\alpha^2}\cosh(\sqrt{2\omega\mathrm{i}}(-1+d))\\&\cdot\cosh(\sqrt{2\omega\mathrm{i}+\alpha^2}d)-\sqrt{2\omega\mathrm{i}}\sinh(\sqrt{2\omega\mathrm{i}}(-1+d))\sinh(\sqrt{2\omega\mathrm{i}+\alpha^2}d)\Big).\end{aligned} \tag{27}$$

The corresponding volume flow rate is obtained as

$$\begin{aligned}Q=&Q_x+\mathrm{i}Q_y=2\int_{-1}^{0}\chi(z)\mathrm{d}z\\=&\frac{2B_3}{\sqrt{2\omega\mathrm{i}+\alpha^2}}(\sinh(\sqrt{2\omega\mathrm{i}+\alpha^2}(-1+d))+\sinh(\sqrt{2\omega\mathrm{i}+\alpha^2}))+\frac{2B_4}{\sqrt{2\omega\mathrm{i}+\alpha^2}}\end{aligned}$$

$$\cdot(\cosh(\sqrt{2\omega\mathrm{i}+\alpha^2}(-1+d))-\cosh(\sqrt{2\omega\mathrm{i}+\alpha^2}))+\frac{2\lambda}{(1-(\alpha^2+2\omega\mathrm{i})\lambda^2)\cosh(1/\lambda)}$$

$$\cdot\left(K^2\sinh D\cosh\left(\frac{d}{\lambda}\right)-(2K^2-\zeta)\sinh D+(K^2-\zeta)\sinh\left(\frac{1}{\lambda}\right)\right)+\frac{2B_1}{\sqrt{2\omega\mathrm{i}}}$$

$$\cdot\sinh(\sqrt{2\omega\mathrm{i}}(1-d))+\frac{2\lambda\sinh D}{(2\omega\mathrm{i}\lambda^2-1)\cosh(1/\lambda)}\left(K^2\cosh\left(\frac{d}{\lambda}\right)+\zeta-K^2\right)+\frac{2K^2d}{(2\omega\mathrm{i}+\alpha^2)\lambda^2}. \quad (28)$$

3 Results and discussion

In the previous section, we have presented the theoretical analysis of the rotating EOF in a soft microchannel. The analytical solutions for the EDL electrostatic potential, axial and transverse velocities, and the volume flow rate are derived. These solutions depend greatly on the corresponding dimensionless parameters defined above. In this section, to further discuss the obtained results, the ranges of the above mentioned parameters should be given first. Physically, the fluid density is $\rho^*=10^3$ kg/m^3, the dynamic viscosity of the Newtonian fluid is $\mu^*=10^{-3}$ kg/(m·s), the height of the microchannel is $2h=200$ μm, and the rotating frequency Ω is from 0 rps to 10^3 rps. Therefore, the dimensionless frequency ω changes from 0 to 10. In addition, the ranges of the other corresponding parameters are presented from a relevant paper[45]. For example, the nondimensional drag coefficient α changes from 1 to 10, the dimensionless PEL thickness d changes from 0 to 0.1, the dimensionless EDL thickness λ is set to 0.1, and the equivalent EDL thickness λ_{FCL} changes from 0.1 to 0.5. It needs to point out that the relation $d\leqslant\lambda\leqslant\lambda_{\mathrm{FCL}}$ should be satisfied to guarantee the validity of the low zeta potential approximation[46].

Figure 2 depicts the distributions of the dimensionless electrical potential ψ with d and λ_{FCL}. From Fig. 2(a), it is evident that the electrical potential ψ increases with d. The possible reason may be that the PEL includes a particular kind of ion and increases the electrical potential in the entire system, which will be more prominent for larger d. However, Fig. 2(b) shows that larger λ_{FCL} will lead to smaller ψ since larger λ_{FCL} implies a weaker FCL ions effect according to the equation $\lambda^*_{\mathrm{FCL}}=(\varepsilon_0\varepsilon_{\mathrm{r}}k_{\mathrm{B}}T/(Ne^2mZ))^{1/2}$.

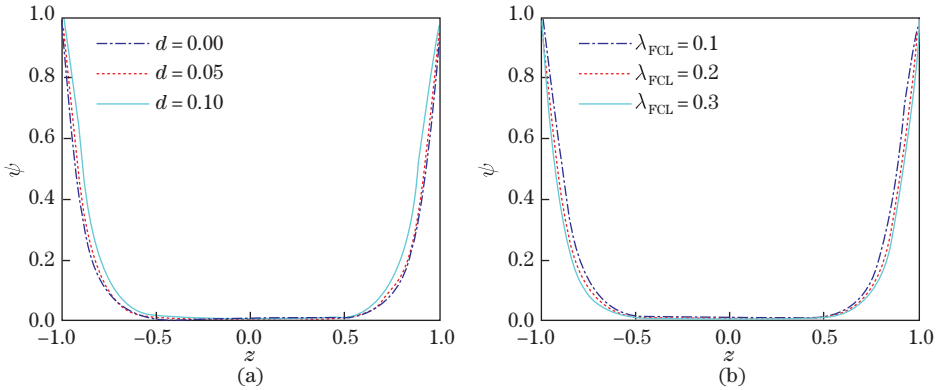

Fig. 2 Variations of the electrical potential ψ with the dimensionless height z for different values of d ($\lambda=0.1$ and $\alpha=10$), (a) $\lambda_{\mathrm{FCL}}=0.1$ and (b) $d=0.1$

The variations of the axial and transverse velocities u and v for different d and λ_{FCL} are shown in Fig. 3. Figures 3(a) and 3(b) imply that the thicker the PEL thickness d, the larger the velocities u and v, when the equivalent EDL thickness λ_{FCL} is relatively small ($\lambda_{\mathrm{FCL}}=0.1$). However, a reversed trend is obtained from Figs. 3(c) and 3(d) for the larger value of λ_{FCL} ($\lambda_{\mathrm{FCL}}=0.3$). This is due to the twofold effects of the FCL layer on the electrokinetic

transport. Firstly, the fixed FCL ions increase the electrical potential ψ and the EOF velocity due to the increasing electroosmotic force. Secondly, there will be a resistive force within the FCL imparted by the grafted polyelectrolyte, leading to the decrease in the EOF velocity. For smaller $\lambda_{\rm FCL}$ (see Figs. 3(a) and 3(b)), the concentration of the fixed FCL ions is larger. In this case, the increasing effect of the EOF velocity caused by the FCL is dominant over the decreasing effect. Thus, the velocities u and v increase with the FCL thickness d. However, for the larger value of $\lambda_{\rm FCL}$ (see Figs. 3(c) and 3(d)), the resistive force is more prominent due to the smaller concentration of the fixed FCL ions. This implies that the velocities u and v decrease with the increasing FCL thickness d. Moreover, as we have expected, in a special case of our present results when $d = 0$, the velocities u and v for a soft microchannel are exactly the same as the results obtained by Chang and Wang[32] for a rigid parallel plate microchannel.

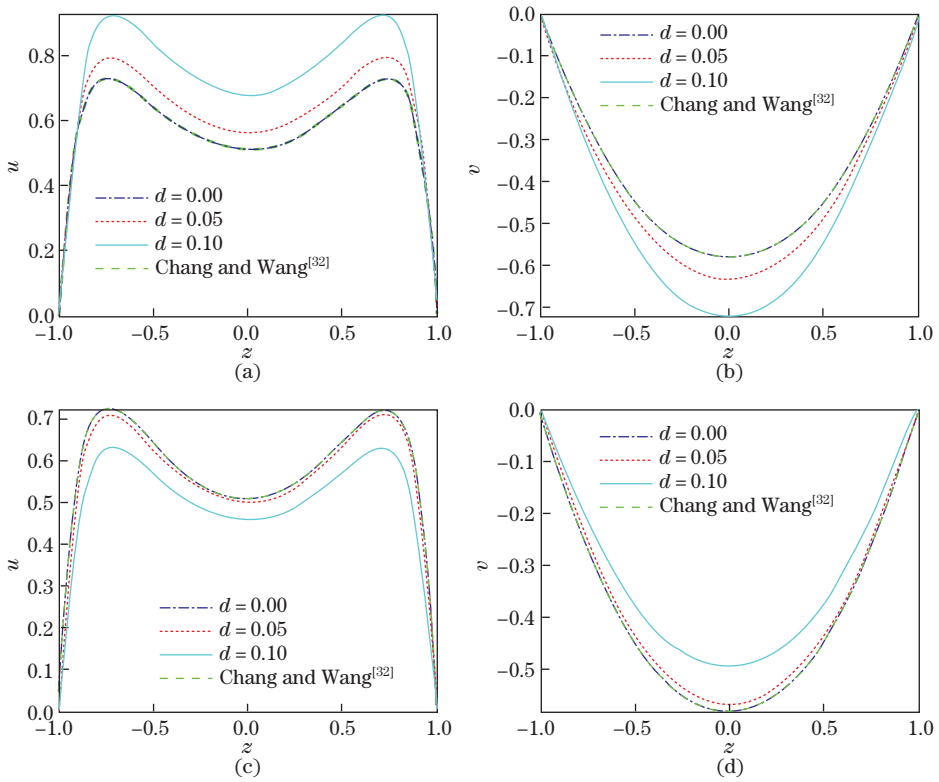

Fig. 3 Velocity variations with the dimensionless height z for different d ($\lambda = 0.1$, $\omega = 1$, and $\alpha = 10$), (a) the velocity u ($\lambda_{\rm FCL} = 0.1$), (b) the velocity v ($\lambda_{\rm FCL} = 0.1$), (c) the velocity u ($\lambda_{\rm FCL} = 0.3$), and (d) the velocity v ($\lambda_{\rm FCL} = 0.3$)

Figure 4 shows the variations of the axial and transverse velocities with the drag coefficient α. Figure 4 shows the increase in the drag coefficient α decreases the velocities u and v. This can be explained that α represents the drag force in the FCL, and larger α implies the larger resistive force, which results in smaller velocities u and v.

Figure 5 depicts distributions of the axial velocity u and the transverse velocity v for different values of the nondimensional rotating frequency ω both in a soft microchannel and in a rigid one. In the legends of Figs. 5(a) and 5(b), the letter S(R) indicates the plots for a soft (rigid) microchannel. We observe that the velocity u decreases with the increase in ω for both soft and rigid channels. From Figs. 5(a) and 5(b), for a prescribed lower rotating frequency ($\omega < 5$), both velocities in the x- and y-axes for a soft channel are smaller than those for a rigid one. However, for a larger rotating frequency ($\omega = 5$), the main stream velocity u far away from the

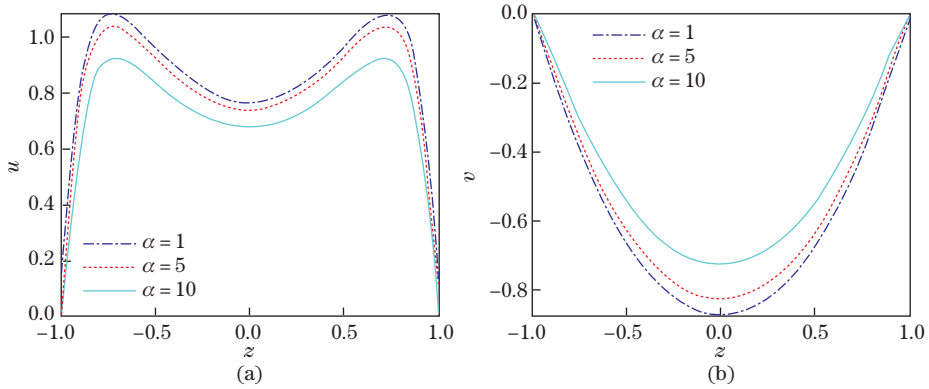

Fig. 4 Velocity variations with the dimensionless height z for different α, (a) the velocity u and (b) the velocity v ($\lambda_{\mathrm{FCL}} = 0.1$, $\lambda = 0.1$, $d = 0.1$, and $\omega = 1$)

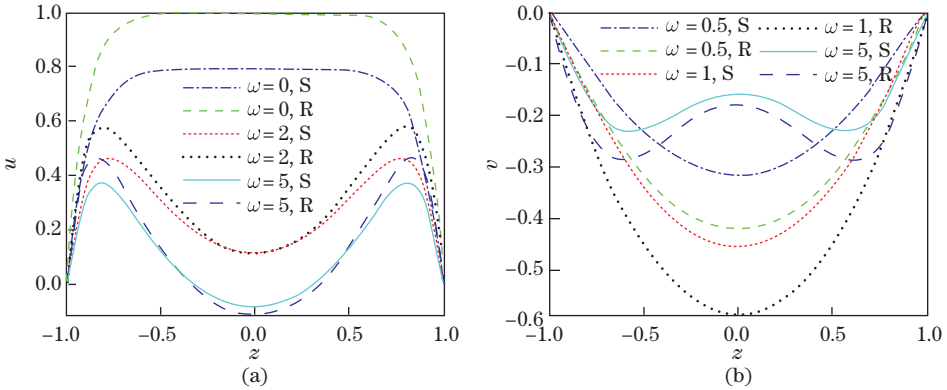

Fig. 5 Velocity variations with the nondimensional rotating angular frequency ω for both soft and rigid microchannels ($\alpha = 10$, $\lambda_{\mathrm{FCL}} = 0.3$, $d = 0.1$, and $\lambda = 0.1$), (a) the velocity u and (b) the velocity v

walls in a soft channel exceeds that in a rigid one. The result is interesting, because in some applications they need the larger EOF velocity. Based on this situation, for a higher rotating frequency in a rotating system, we can use a soft microchannel to enhance the main stream velocity far away from the walls. The reasonable explanation can be that, for a larger rotating frequency ($\omega = 5$), the axial velocity u is suppressed and even becomes negative near the microchannel center. In this case, the maximum value of the axial velocity shifts from the rigid channel center towards the channel boundaries due to the complex interaction between the electrical force and the Coriolis force[32]. However, for a soft microchannel, due to the retardation effect of the FCL, the shift phenomenon of the maximum axial velocity towards the soft microchannel boundaries is confined. In addition, the induced velocity v in the y-axis is not a monotonic function, and it increases with the rotating frequency ω when $\omega < 1$ and decreases with the rotating frequency ω when $\omega > 1$.

We define an angle $\beta = \arctan(Q_y/Q_x)$ to examine the flow rate ratio of the y-axis to the x-axis. Figures 6 and 7 plot the variations of the flow angle β with the rotating frequency ω for different α and d, respectively. One may find from Figs. 6 and 7 that for a smaller rotating frequency $\omega\,(0.001 < \omega < 0.01)$, the flow angle β keeps constant with the increase in ω. However, for larger $\omega\,(0.01 < \omega < 10)$, the flow angle β decreases with ω. Also, from Figs. 6 and 7, we can see that the parameters α and d have negligible effects on β for ω lower than 3. However, when ω is larger than 3, the parameters α and d have adverse effects on β. From

Fig. 7, it is seen that the increase in d increases β, and from Fig. 6, the increase in α decreases β, which can be obtained when ω is larger than 3.

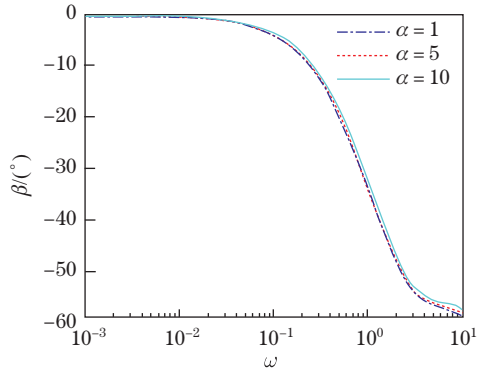

Fig. 6 Variations of $\beta = \arctan(Q_y/Q_x)$ as a function of ω for different α ($\lambda_{\mathrm{FCL}} = 0.1$, $\lambda = 0.1$, and $d = 0.1$)

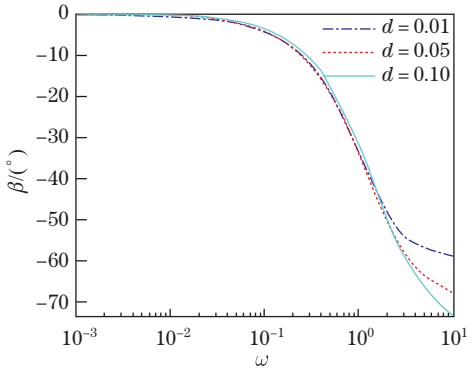

Fig. 7 Variations of $\beta = \arctan(Q_y/Q_x)$ as a function of ω for different d ($\lambda_{\mathrm{FCL}} = 0.5$, $\lambda = 0.1$, and $\alpha = 10$)

4 Conclusions

In the present work, the rotating EOF in the PEL covered parallel plate microchannels is investigated theoretically. After discussing the results, we obtain important conclusions. Firstly, for a smaller equivalent EDL thickness $\lambda_{\mathrm{FCL}}(\lambda_{\mathrm{FCL}} = 0.1)$, a larger value of PEL thickness d leads to larger axial and transverse velocities. However, a reversed trend is obtained for larger $\lambda_{\mathrm{FCL}}(\lambda_{\mathrm{FCL}} = 0.3)$. Secondly, the velocities in both directions decrease with the increase in the drag coefficient α. For lower rotating frequencies ($\omega < 5$) and larger $\lambda_{\mathrm{FCL}}(\lambda_{\mathrm{FCL}} = 0.3)$, both velocities in x- and y-axes for a soft channel are smaller than those for a rigid one. However, for a larger rotating frequency ($\omega = 5$), the velocity u in the x-axis for a soft microchannel exceeds that for a rigid one near the channel center ($\lambda_{\mathrm{FCL}} = 0.3$). Finally, the flow angle β (the flow rate ratio of the y-axis to the x-axis) increases with the FCL thickness d and decreases with the drag coefficient α for a given rotating frequency ω ($\omega > 3$).

References

[1] STONE, H. A., STROOCK, A. D., and AJDARI, A. Engineering flows in small devices: microfluidics toward a lab-on-a-chip. *Annual Review of Fluid Mechanics*, **36**, 381–411 (2004)

[2] LASTER, D. J. and SANTIAGO, J. G. A review of micropumps. *Journal of Micromechanics and Microengineering*, **14**(6), R35–R64 (2004)

[3] GHOSAL, S. Lubrication theory for electro-osmotic flow in a microfluidic channel of slowly varying cross-section and wall charge. *Journal of Fluid Mechanics*, **459**, 103–128 (2002)

[4] RAMON, G. Z. Solute transport under oscillating electro-osmotic flow in a closed-ended cylindrical pore. *Journal of Engineering Mathematics*, **110**(1), 195–205 (2018)

[5] JIAN, Y. J., YANG, L. G., and LIU, Q. S. Time periodic electro-osmotic flow through a microannulus. *Physics of Fluids*, **22**(4), 042001 (2010)

[6] JIAN, Y. J., LIU, Q. S., and YANG, L. G. AC electroosmotic flow of generalized Maxwell fluids in a rectangular microchannel. *Journal of Non-Newton Fluid Mechanics*, **166**, 1304–1314 (2011)

[7] AFONSO, A. M., ALVES, M. A., and PINHO, F. T. Electro-osmotic flow of viscoelastic fluids in microchannels under asymmetric zeta potentials. *Journal of Engineering Mathematics*, **71**(1), 15–30 (2011)

[8] VAN LINEEL, H. T. G., VAN DE POL, F. C. M., and BOUWSTRA, S. A piezoelectric micropump based on micromachining of silicon. *Sensors and Actuators*, **15**(2), 153–167 (1988)

[9] PAMME, N. Magnetism and microfluidics. *Lab on a Chip*, **6**(1), 24–38 (2006)

[10] JANG, J. and LEE, S. S. Theoretical and experimental study of MHD (magnetohydrodynamic) micropump. *Sensors and Actuators A*: *Physical*, **80**(1), 84–89 (2000)

[11] RIVERO, M. and CUEVAS, S. Analysis of the slip condition in magnetohydrodynamic (MHD) micropumps. *Sensors and Actuators B*: *Chemical*, **166**, 884–892 (2012)

[12] BUREN, M. D. L., JIAN, Y. J., and CHANG, L. Electromagnetohydrodynamic flow through a microparallel channel with corrugated walls. *Journal of Physics D*: *Applied Physics*, **47**(42), 425501 (2014)

[13] SI, D. Q. and JIAN, Y. J. Electromagnetohydrodynamic (EMHD) micropump of Jeffrey fluids through two parallel microchannels with corrugated walls. *Journal of Physics D*: *Applied Physics*, **48**(8), 085501 (2015)

[14] ZHAO, G. P., JIAN, Y. J., CHANG, L., and BUREN, M. D. L. Magnetohydrodynamic flow of generalized Maxwell fluids in a rectangular micropump under an AC electric field. *Journal of Magnetism and Magnetic Materials*, **387**, 111–117 (2015)

[15] JIAN, Y. J. and CHANG, L. Electromagnetohydrodynamic (EMHD) micropumps under a spatially non-uniform magnetic field. *AIP Advances*, **5**(5), 057121 (2015)

[16] JIAN, Y. J. Transient MHD heat transfer and entropy generation in a microparallel channel combined with pressure and electroosmotic effects. *International Journal of Heat and Mass Transfer*, **89**, 193–205 (2015)

[17] WANG, L., JIAN, Y. J., LIU, Q. S., LI, F. Q., and CHANG, L. Electromagnetohydrodynamic flow and heat transfer of third grade fluids between two micro-parallel plates. *Colloids and Surfaces A*: *Physicochemical and Engineering Aspects*, **494**, 87–94 (2016)

[18] JIAN, Y. J., SI, D. Q., CHANG, L., and LIU, Q. S. Transient rotating electromagneto hydrodynamic micropumps between two infinite microparallel plates. *Chemical and Engineering Science*, **134**, 12–22 (2015)

[19] RANJIT, N. K. and SHIT, G. C. Joule heating effects on electromagnetohydrodynamic flow through a peristaltically induced micro-channel with different zeta potential and wall slip. *Physica A*: *Statistical Mechanics and Its Applications*, **482**, 458–476 (2017)

[20] SHIT, G. C., MONDAL, A., SINHA, A., and KUNDU, P. K. Electro-osmotically driven MHD flow and heat transfer in micro-channel. *Physica A*: *Statistical Mechanics and Its Applications*, **449**, 437–454 (2016)

[21] WEINERT, F. M., WUHR, M., and BRAUNA, D. Light driven microflow in ice. *Applied Physics Letters*, **94**(11), 113901 (2009)

[22] YEO, L. Y. and FRIEND, J. R. Surface acoustic wave microfluidics. *Annual Review of Fluid Mechanics*, **46**, 379–406 (2014)

[23] DAS, S., CHAKRABORTY, S., and MITYA, S. K. Redefining electrical double layer thickness in narrow confinements: effect of solvent polarization. *Physics Review E*, **85**(5), 051508 (2012)

[24] MANZ, A., GRABER, N., and WIDMER, H. M. Miniaturized total chemical analysis systems: a novel concept for chemical sensing. *Sensors and Actuators B*: *Chemical*, **1**, 244–248 (1990)

[25] KUMAR, M. S., SANDEEP, N., and KUMAR, B. R. Three-dimensional magnetohydrodynamic rotating flow past a stretched surface with cross diffusion. *Chinese Journal of Physics*, **55**(6), 2407–2421 (2017)

[26] HAYAT, T., ZAHIR, H., ALSAEDI, A., and AHMAD, B. Heat transfer analysis on peristaltic transport of Ree-Eyring fluid in rotating frame. *Chinese Journal of Physics*, **55**(5), 1894–1907 (2017)

[27] GORKIN, R., PARK, J., SIEGRIST, J., AMASIA, M., LEE, B. S., PARK, J. M., and CHO, Y. K. Centrifugal microfluidics for biomedical applications. *Lab on a Chip*, **10**(14), 1758–1773 (2010)

[28] WANG, G. J., HSU, W. H., CHANG, Y. Z., and YANG, H. Centrifugal and electric field forces dual-pumping CD-like microfluidic platform for biomedical separation. *Biomedical Microdevices*, **6**(1), 47–53 (2004)

[29] MARTINEZ-DUARTE, R., GORKIN, R. A., ABI-SAMRAB, K., and MADOU, M. J. The integration of 3D carbon-electrode dielectrophoresis on a CD-like centrifugal microfluidic platform. *Lab on a Chip*, **10**(1), 1030–1043 (2010)

[30] BOETTCHER, M., JAEGER, M., RIEGGER, L., DUCREE, J., ZENGERLE, R., and DUSCHL, C. Lab-on-chip-based cell separation by combining dielectrophoresis and centrifugation. *Biophysical Reviews Letters*, **1**(4), 443–451 (2006)

[31] DUFFY, D. C., GILLIS, H. L., LIN, J., SHEPPARD, N. F., and KELLOGG, G. J. Microfabricated centrifugal microfluidic systems: characterization and multiple enzymatic assays. *Analytical Chemistry*, **71**(20), 4669–4678 (1999)

[32] CHANG, C. C. and WANG, C. Y. Rotating electro-osmotic flow over a plate or between two plates. *Physical Review E*, **84**, 056320 (2011)

[33] SI, D. Q., JIAN, Y. J., CHANG, L., and LIU, Q. S. Unsteady rotating electroosmotic flow through a slit microchannel. *Journal of Mechanics*, **32**(5), 603–611 (2016)

[34] GHESHLAGHI, B., NAZARIPOOR, H., KUMAR, A., and SADRZADEH, M. Analytical solution for transient electroosmotic flow in a rotating microchannel. *RSC Advances*, **6**(21), 17632–17641 (2016)

[35] XIE, Z. Y. and JIAN, Y. J. Rotating electroosmotic flow of power-law fluids at high zeta potentials. *Colloids and Surfaces A*: *Physicochemical and Engineering Aspects*, **461**, 231–239 (2014)

[36] NG, C. O. and QI, C. Electro-osmotic flow in a rotating rectangular microchannel. *Proceedings of The Royal Society A—Mathematical Physical and Engineering Sciences*, **471**(2179), 20150200 (2015)

[37] SHIT, G. C., MONDAL, A., SINHA, A., and KUNDU, P. K. Effects of slip velocity on rotating electro-osmotic flow in a slowly varying micro-channel. *Colloids and Surfaces A*: *Physicochemical and Engineering Aspects*, **489**, 249–255 (2016)

[38] OHSHIMA, H. Electrical phenomena in a suspension of soft particles. *Soft Matter*, **8**(13), 3511–3514 (2012)

[39] BARBATI, A. C. and KIRBY, B. J. Soft diffuse interfaces in electrokinetics — theory and experiment for transport in charged diffuse layers. *Soft Matter*, **8**(41), 10598–10613 (2012)

[40] XING, J. N. and JIAN, Y. J. Steric effects on electroosmotic flow in soft nanochannels. *Meccanica*, **53**(1/2), 135–144 (2018)

[41] DONATH, E. and VOIGT, E. Streaming current and streaming potential on structured surfaces. *Journal of Colloid and Interface Science*, **109**(1), 122–139 (1986)

[42] ZHANG, H., TIAN, Y., and JIANG, L. From symmetric to asymmetric design of bio-inspired smart single nanochannels. *Chemical Communications*, **49**(86), 10048–10063 (2013)

[43] KALMAN, E. B., VLASSIOUK, I., and SIWY, Z. Nanofluidic bipolar transistors. *Advanced Materials*, **20**(2), 293–297 (2008)

[44] MATIN, M. H. and OHSHIMA, H. Combined electroosmotically and pressure driven flow in soft nanofluidics. *Journal of Colloid and Interface Science*, **460**, 361–369 (2015)

[45] CHANDA, S., SINHA, S., and DAS, S. Streaming potential and electroviscous effects in soft nanochannels: towards designing more efficient nanofluidic electrochemomechanical energy converters. *Soft Matter*, **10**(38), 7558–7568 (2014)

[46] CHEN, G. and DAS, S. Streaming potential and electroviscous effects in soft nanochannels beyond Debye-Hückel linearization. *Journal of Colloid and Interface Science*, **445**, 357–363 (2015)

[47] HOSHYARGAR, V., KHORAMI, A., ASHRAFIZADEH, S. N., and SADEGHI, A. Solute dispersion by electroosmotic flow through soft microchannels. *Sensors and Actuators B*: *Chemical*, **255**, 3585–3600 (2017)

[48] SADEGHI, A. Theoretical modeling of electroosmotic flow in soft microchannels: a variational approach applied to the rectangular geometry. *Physics of Fluids*, **30**(3), 032004 (2018)

[49] PANG, Y., KIM, H., LIU, Z. M., and STONE, H. A. A soft microchannel decreases polydispersity of droplet generation. *Lab on a Chip*, **14**(20), 4029–4034 (2014)

[50] LIU, Z. M., WANG, X., CAO, R. T., and PANG, Y. Droplet coalescence at microchannel intersection chambers with different shapes. *Soft Matter*, **12**(26), 5797–5807 (2016)